Title

Loss of dual leucine zipper kinase signaling is protective in animal models of neurodegenerative disease

Journal

Science Translational Medicine, 9(403)

ISSN

1946-6234

Authors

Le Pichon, Claire E
Meilandt, William J
Dominguez, Sara
et al.

Publication Date

2017-08-16

DOI

10.1126/scitranslmed.aag0394

Peer reviewed

NEURODEGENERATIVE DISEASE

Loss of dual leucine zipper kinase signaling is protective in animal models of neurodegenerative disease

Claire E. Le Pichon,[1*†] William J. Meilandt,[1*‡] Sara Dominguez,[1] Hilda Solanoy,[1§] Han Lin,[1] Hai Ngu,[2] Alvin Gogineni,[3] Arundhati Sengupta Ghosh,[1] Zhiyu Jiang,[1] Seung-Hye Lee,[1] Janice Maloney,[1] Vineela D. Gandham,[3] Christine D. Pozniak,[1] Bei Wang,[1‖] Sebum Lee,[4] Michael Siu,[5] Snahel Patel,[5] Zora Modrusan,[6] Xingrong Liu,[7] York Rudhard,[8] Miriam Baca,[2] Amy Gustafson,[9] Josh Kaminker,[10] Richard A. D. Carano,[3] Eric J. Huang,[4,11] Oded Foreman,[2] Robby Weimer,[3] Kimberly Scearce-Levie,[1§] Joseph W. Lewcock[1‡§]

Hallmarks of chronic neurodegenerative disease include progressive synaptic loss and neuronal cell death, yet the cellular pathways that underlie these processes remain largely undefined. We provide evidence that dual leucine zipper kinase (DLK) is an essential regulator of the progressive neurodegeneration that occurs in amyotrophic lateral sclerosis and Alzheimer's disease. We demonstrate that DLK/c-Jun N-terminal kinase signaling was increased in mouse models and human patients with these disorders and that genetic deletion of DLK protected against axon degeneration, neuronal loss, and functional decline in vivo. Furthermore, pharmacological inhibition of DLK activity was sufficient to attenuate the neuronal stress response and to provide functional benefit even in the presence of ongoing disease. These findings demonstrate that pathological activation of DLK is a conserved mechanism that regulates neurodegeneration and suggest that DLK inhibition may be a potential approach to treat multiple neurodegenerative diseases.

INTRODUCTION

The progressive degeneration of neurons underlies a range of diseases, such as amyotrophic lateral sclerosis (ALS) and Alzheimer's disease (AD), for which there are no disease-modifying treatments. Although recent advances in human genetics have identified causative factors in neurodegenerative disease (*1*, *2*), the pathways induced within neurons in response to these triggers are still poorly understood. Furthermore, most clinical cases of ALS and AD are sporadic, with no clear definable cause. A better understanding of how neurons respond to chronic stress may reveal common links between neurodegenerative diseases and suggest therapeutic avenues to modify disease progression regardless of the initial insult.

Recent work has identified the neuron-enriched kinase dual leucine zipper kinase (DLK) as an integrator of many types of neuronal injury, suggesting that this kinase may be a conserved driver of neuronal degeneration (*3*–*8*). DLK is required for initiation of the c-Jun N-terminal kinase (JNK)–dependent stress response in neurons and broadly regulates injury-induced transcriptional changes (*3*, *5*). Neurons lacking DLK expression are protected against axon degeneration and neuronal apoptosis, both during healthy development and in response to diverse neuronal insults (*3*–*8*). DLK also supports regeneration in invertebrate models and in permissive environments in mouse, such as peripheral nerve injury (*5*, *9*–*12*). In all of these scenarios, DLK functions as an injury sensor that regulates the neuronal stress response, with the adoption of proapoptotic and proregenerative outcomes depending on the specific cellular context (*5*). The central role of DLK in response to neuronal injury suggests that pharmacological inhibition of this kinase may be beneficial in chronic neurodegenerative disease, but this has yet to be tested experimentally in progressive disease models.

Inhibition of JNK pathway signaling downstream of DLK has been shown to slow neuronal degeneration in some contexts (*13*), but it has proved challenging to generate brain-penetrant compounds that safely and effectively target specific JNK isoforms (*14*). DLK inhibition may have similar benefits, and the development of selective, brain-penetrant DLK inhibitors suggests that it represents a more tractable therapeutic target (*15*, *16*). Here, we demonstrate that loss or inhibition of DLK signaling rapidly reversed the neuronal stress response in several chronic neurodegenerative disease models even if initiated after disease onset. Halting this stress response prolonged neuronal survival, preserved synapses, and improved cognitive and motor function in mouse models of ALS and AD.

RESULTS

The JNK pathway is activated in central nervous system tissues from mouse models and patients with ALS or AD

To ascertain whether activation of the DLK/JNK pathway contributes to chronic neurodegenerative disease, we first examined whether aberrant

[1]Department of Neuroscience, Genentech Inc., 1 DNA Way, South San Francisco, CA 94080, USA. [2]Department of Pathology, Genentech Inc., 1 DNA Way, South San Francisco, CA 94080, USA. [3]Department of Biomedical Imaging, Genentech Inc., 1 DNA Way, South San Francisco, CA 94080, USA. [4]Department of Pathology, University of California, San Francisco, San Francisco, CA 94143, USA. [5]Department of Discovery Chemistry, Genentech Inc., 1 DNA Way, South San Francisco, CA 94080, USA. [6]Department of Molecular Biology, Genentech Inc., 1 DNA Way, South San Francisco, CA 94080, USA. [7]Department of Drug Metabolism and Pharmacokinetics, Genentech Inc., 1 DNA Way, South San Francisco, CA 94080, USA. [8]In Vitro Pharmacology, Evotec AG, Manfred Eigen Campus, 22419 Hamburg, Germany. [9]Department of Biochemical and Cellular Pharmacology, Genentech Inc., 1 DNA Way, South San Francisco, CA 94080, USA. [10]Department of Bioinformatics, Genentech Inc., 1 DNA Way, South San Francisco, CA 94080, USA. [11]Pathology Service 113B, San Francisco Veterans Affairs Medical Center, San Francisco, CA 94121, USA.
*These authors contributed equally to this work.
†Present address: Eunice Kennedy Shriver National Institute of Child Health and Human Development, National Institutes of Health, Bethesda, MD 20892, USA.
‡Corresponding author. Email: lewcock@dnli.com (J.W.L.); meilandt.william@gene.com (W.J.M.)
§Present address: Denali Therapeutics, 151 Oyster Point Boulevard, South San Francisco, CA 94080, USA.
‖Present address: Department of Molecular Biology and Genetics, Weill Institute for Cell and Molecular Biology, Cornell University, 435 Weill Hall, Ithaca, NY 14853, USA.

JNK signaling occurs in the context of progressive neurodegeneration. Phosphorylation of both JNK and the downstream target c-Jun was examined, with a particular focus on phosphorylated c-Jun (p-c-Jun) because it is a specific marker of stress-induced JNK activity in neurons (*4*, *5*, *17*–*20*). In the SOD1^{G93A} transgenic mouse model of familial ALS (*21*, *22*), we found an age-dependent increase in p-c-Jun–positive cells in lumbar spinal cord of SOD1^{G93A} transgenic mice between 9 and 14 weeks of age, with little staining in nontransgenic (nonTg) littermate controls (Fig. 1, A and B), consistent with previous reports (*17*, *18*). Costaining for the neuronal marker NeuN (Fig. 1C) revealed that p-c-Jun staining was almost entirely neuronal, with 94 of 100 p-c-Jun–positive cells also expressing NeuN (fig. S2F). Moreover, p-c-Jun costained with choline acetyltransferase (ChAT)–positive motor neurons, which are susceptible to death in this ALS disease mouse model (fig. S1A). *Dlk* mRNA localized to cells expressing the pan-neuronal marker *Tubb3* (Fig. 1D and fig. S1B) and the motor neuron marker *Chat* (fig. S1C), implying that DLK activity could be driving the phosphorylation of c-Jun in neurons. The number of p-c-Jun–positive cells was also increased in the cortex of a second ALS model, the TDP-43^{A315T} transgenic mouse (Fig. 1, H and I) (*23*). Many components of the JNK signaling pathway, including phosphorylated JNK (p-JNK), p-c-Jun, total JNK, and total c-Jun, were increased in lumbar spinal cord lysates from patients with sporadic ALS (Fig. 1, E to G), suggesting that activation of the JNK pathway occurs in the human disease and is not limited to ALS caused by SOD1 mutations.

JNK pathway activity was also elevated in two transgenic mouse strains that model specific aspects of AD, PS2APP and Tau^{P301L} (*24*–*26*), at ages greater than 6 months (Fig. 2, A to D, and fig. S2, A to D). p-c-Jun was detected almost exclusively within NeuN-positive cells in both PS2APP mice and Tau^{P301L} mice (fig. S2, E and F), indicating that the aberrant JNK pathway activity was similarly limited to neurons in these models. In postmortem central nervous system (CNS) tissues from patients with either early-stage AD or confirmed AD, p-c-Jun immunostaining was significantly elevated in hippocampal neurons (Fig. 2, E and F; $P < 0.01$), consistent with previous findings (*27*, *28*). To determine whether the presence of aberrant JNK activity correlated with the extent of disease pathology, we examined p-c-Jun, total c-Jun, and p-JNK in control, early-stage AD, and confirmed AD patient superior frontal gyrus, a brain region affected predominantly in the later stages of AD (*29*). In these samples, increased JNK activity was observed only in confirmed AD but not in early AD postmortem brain samples (Fig. 2, G to I). Expression of p-JNK and p-c-Jun in these samples correlated well with the presence of phosphorylated pathogenic Tau (pS202 and pS396/S404) (Fig. 2, G to I and fig. S2, G and H), suggesting that stress-induced JNK activation occurs specifically in brain regions where disease pathology is present.

Loss of DLK reduces JNK activity in animal models of neurodegenerative disease

During development or after acute neuronal injury, DLK is required for stress-induced JNK pathway activation and phosphorylation of c-Jun in neurons (*3*–*5*, *10*). To determine whether this was the case in the context of progressive neurodegeneration, we crossed SOD1^{G93A}, PS2APP, and Tau^{P301L} mice with a DLK conditional knockout/CAAGS-Cre^{ERT} (DLK^{cKO}) mouse (*4*). In this model, *Dlk* excision could be achieved in adult mice by tamoxifen-induced Cre recombination, a strategy that avoids potential developmental phenotypes and more accurately models systemic DLK inhibitor treatment. In SOD1^{G93A};DLK^{cKO} mice administered tamoxifen from 4 to 7 weeks of age, the *Dlk* recombination efficiency was ~66 to 80% in lumbar spinal cord, as measured by quantitative polymerase chain reaction (qPCR) (fig. S3A). Even this incomplete removal of DLK was able to reduce the number of p-c-Jun–positive cells per section of the spinal cord by 47% in SOD1^{G93A};DLK^{cKO} mice compared to SOD1^{G93A};DLK^{WT} littermates that lack the Cre^{ERT} transgene at 14 weeks of age (Fig. 3, A and B; $P < 0.0001$).

In the PS2APP and Tau^{P301L} mice, tamoxifen treatment was initiated at ~10 weeks of age and brain tissues were collected at 9 months of age, after significant AD-related pathology had developed. Deletion of *Dlk* reduced cortical DLK protein in both PS2APP;DLK^{cKO} and Tau^{P301L};DLK^{cKO} mice (~75 to 81%; Fig. 3, C, D, G, and H; $P < 0.0001$). This reduction in DLK expression was sufficient to significantly reduce cortical p-c-Jun (~41 to 48%) and total c-Jun (~30%; Fig. 3, C, D, G, and H; $P < 0.0001$) by Western blotting in both PS2APP;DLK^{cKO} and Tau^{P301L};DLK^{cKO} mice. The reduction in total c-Jun aligned with the previous finding that inhibition of c-Jun phosphorylation reduces total c-Jun expression (*30*). To confirm that the reductions in p-c-Jun resulted from reduced DLK pathway activation, we measured the activity of two upstream components of the DLK/JNK pathway, MKK4 (mitogen-activated protein kinase kinase 4) and JNK. Because neurons display high basal activation of JNK and MKK4 that is not stress-dependent or affected by DLK (*4*), less robust changes were observed in these pathway markers after *Dlk* deletion. Small but significant reductions in p-JNK (~11 to 18%) were observed in both models [Fig. 3, D ($P < 0.05$) and H ($P < 0.01$)], whereas phosphorylated MKK4 (p-MKK4) was reduced in PS2APP;DLK^{cKO} mice by ~30% but was unchanged in Tau^{P301L};DLK^{cKO} mice [Fig. 3, C and D ($P < 0.01$), and G and H]. Immunostaining for p-c-Jun confirmed the reductions found by Western blotting: the average number of p-c-Jun–positive cells per square millimeter was significantly reduced throughout the brain in both PS2APP;DLK^{cKO} mice (by 69%; $P < 0.0001$) and Tau^{P301L};DLK^{cKO} mice (by 45%; Fig. 3, E, F, I, and J; $P < 0.0001$). Together, these results demonstrate that loss of DLK reduced stress-induced activation of the JNK pathway in three independent animal models of chronic neurodegenerative disease.

Loss of DLK is neuroprotective in SOD1^{G93A} transgenic mice

We next examined the impact of DLK removal on motor neuron survival by comparing the number of spinal cord motor neurons at 14 weeks of age in SOD1^{G93A};DLK^{WT} mice versus SOD1^{G93A};DLK^{cKO} mice. Whereas SOD1^{G93A}mice with normal DLK expression showed the expected 40% loss of ChAT-positive neurons compared to nonTg littermates, the SOD1^{G93A};DLK^{cKO} mice only lost 13% of ChAT-positive cells (Fig. 4, A and B; $P < 0.001$). To determine whether motor neuron axons were also protected in SOD1^{G93A};DLK^{cKO} mice, we examined total axonal lumen area in cross sections of sciatic nerve. On the basis of the progression of axon degeneration pathology in SOD1^{G93A} mice (*31*), this end point provided the most robust measure at this age (14 weeks), because a significant decrease in axon number has not yet occurred (fig. S3B). Consistent with previous reports, axonal lumen area was decreased in SOD1^{G93A} mice, corresponding to the initial phase of axon degeneration (Fig. 4, C and D; $P < 0.001$). A significant rescue in axonal lumen area was observed in SOD1^{G93A};DLK^{cKO} mice (Fig. 4, C and D), suggesting that *Dlk* deletion was sufficient to elicit axonal protection. SOD1^{G93A};DLK^{cKO} animals also showed significant reductions in both ionized calcium binding adaptor molecule 1 (Iba1)–positive microglia and glial fibrillary acidic protein (GFAP)–positive astrocytes (Fig. 4, E and F, and fig. S3, C and D; $P < 0.0001$ and $P < 0.01$, respectively). Because DLK expression is enriched in neurons compared to glia (Fig. 1D and fig. S1B) (*32*), the reduction in microglial and astrocytic activation suggested that unhealthy neurons may be able to stimulate gliosis.

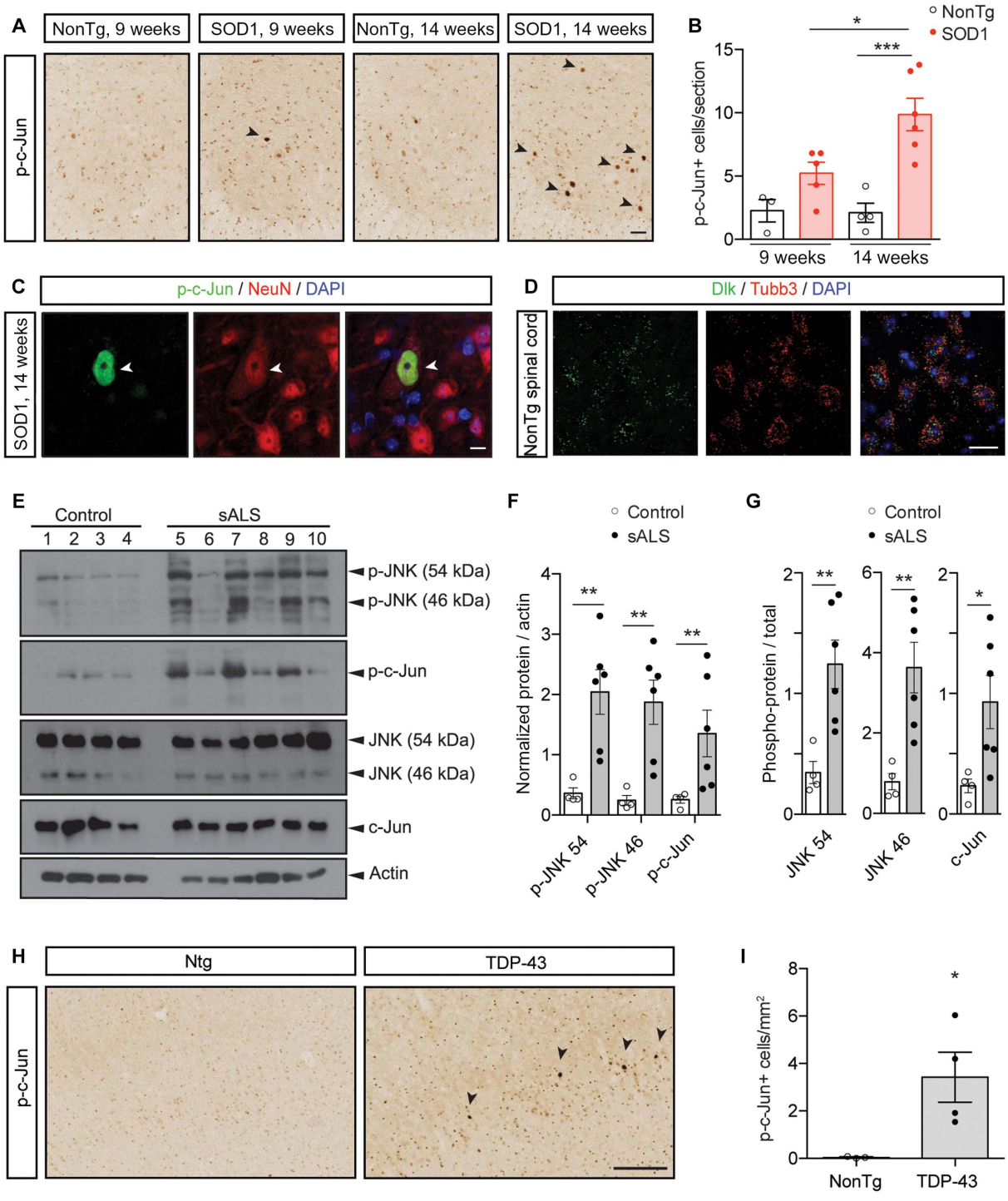

Fig. 1. Aberrant JNK pathway activation in mouse models of ALS and in spinal cord tissue from patients with sporadic ALS. (**A**) Representative images of p-c-Jun immunostaining in nonTg and SOD1^{G93A} mouse spinal cords at 9 and 14 weeks of age. Black arrowheads highlight p-c-Jun–positive nuclei. Scale bar, 40 μm. (**B**) Mean number of p-c-Jun–positive cells per section in spinal cords from SOD1^{G93A} mice at 9 and 14 weeks of age. *$P < 0.05$ and ***$P < 0.001$. (**C**) Representative double staining for p-c-Jun (green), NeuN (red), and DAPI (4′,6-diamidino-2-phenylindole)–positive nuclei (blue) in 14-week-old SOD1^{G93A} mouse spinal cord tissue. White arrowhead points to a NeuN-positive motor neuron. Scale bar, 10 μm. (**D**) *Dlk* (green) expression colocalizes with *Tubb3* (red) by in situ hybridization in nonTg mouse spinal cord. Scale bar, 50 μm. (**E** to **G**) p-JNK and p-c-Jun in lumbar spinal cord lysates from patients with sporadic ALS (sALS). (E) Western blot of p-JNK and p-c-Jun in spinal cord lysates from patients with sALS. (F) p-JNK (54- and 46-kDa isoforms) and p-c-Jun are elevated in spinal cord tissue from sALS patients versus healthy controls. **$P = 0.0095$, two-tailed Mann-Whitney test. (G) Ratios of phosphoprotein to total protein for JNK 54 kDa (JNK 54), JNK 46 kDa (JNK 46), and c-Jun are elevated in spinal cord tissue from sALS patients versus healthy controls. **$P = 0.0095$ and *$P = 0.0190$, Mann-Whitney test. (**H** and **I**) Staining for p-c-Jun in brain cortical tissue from TDP-43^{A315T} transgenic mice, a model of ALS. (H) Representative images of p-c-Jun staining in the cortex of nonTg (left) and TDP-43^{A351T} transgenic littermates (right). Scale bar, 100 μm. (I) Mean number of cortical p-c-Jun–positive cells in TDP-43^{A351T} transgenic and nonTg littermates. *$P < 0.05$, two-tailed Student's *t* test.

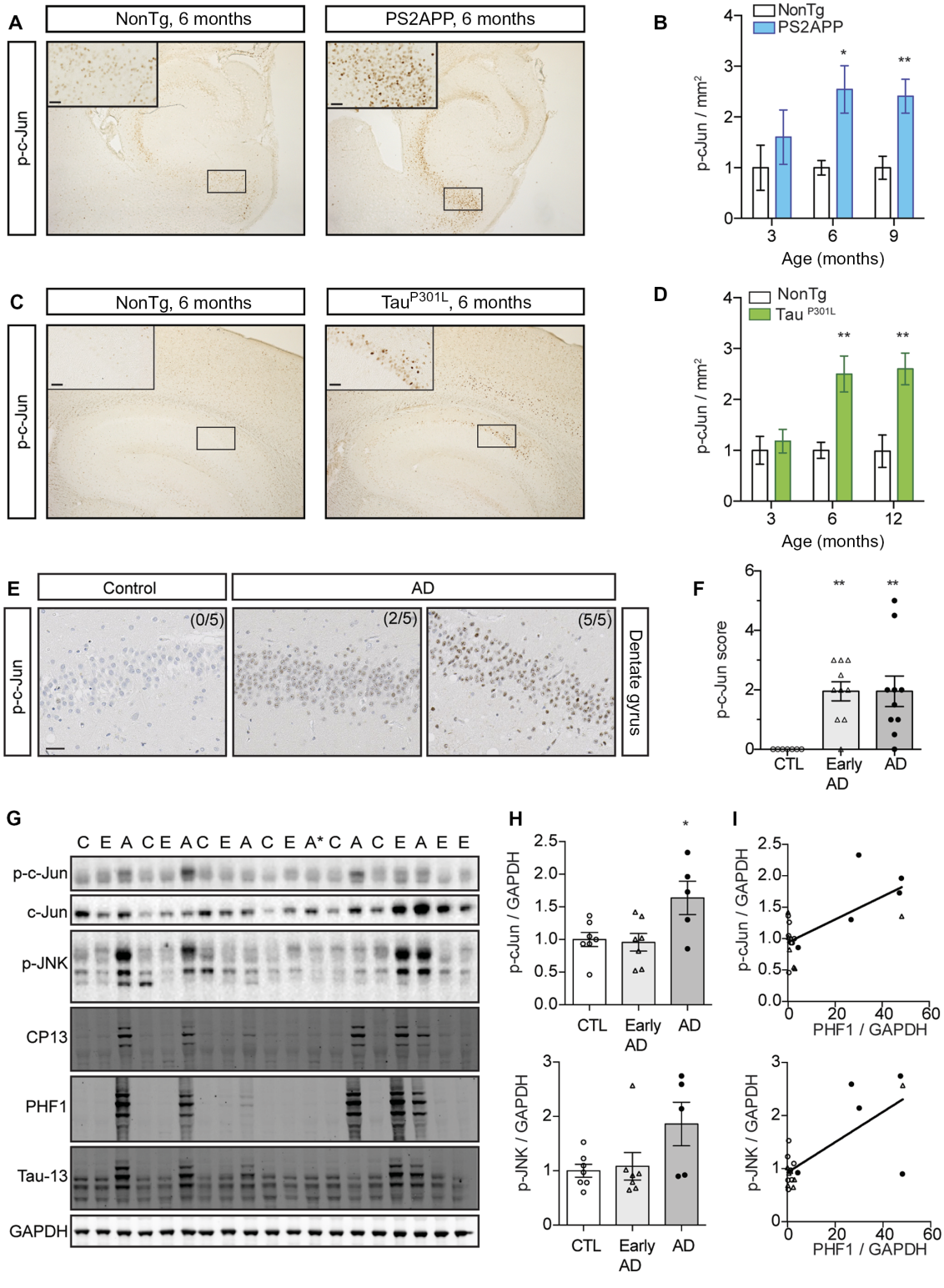

Fig. 2. Aberrant JNK pathway activity in AD mouse models and in samples from patients with AD. (**A**) Representative images of p-c-Jun staining in the ventral hippocampus of 6-month-old nonTg and PS2APP transgenic mice. Boxed regions are high-magnification insets from the subiculum. Scale bars, 40 μm. (**B**) Quantification of p-c-Jun staining in hippocampal tissue from PS2APP versus nonTg littermates. *P < 0.05 and **P < 0.01, two-tailed Student's t test; n = 3 to 6 per group and age. (**C**) Representative images of p-c-Jun staining in dorsal hippocampus of 6-month-old nonTg and Tau^{P301L} transgenic mice. Boxed regions are high-magnification insets from the subiculum/hippocampal CA1 region of the mouse brain. Scale bars, 40 μm. (**D**) Number of hippocampal p-c-Jun–positive cells per square millimeter of tissue from Tau^{P301L} transgenic versus nonTg littermates. *P < 0.05, two-tailed Student's t test; n = 4 to 6 per group and age. (**E**) Representative images of p-c-Jun staining in dentate gyrus of AD patient and age-matched control autopsy brain tissue. p-c-Jun quantification scores noted as (0 to 5 of 5) (see Supplementary Materials and Methods). Scale bar, 40 μm. (**F**) p-c-Jun scores for human hippocampal sections from age-matched controls (CTL) and patients with early-stage AD (early AD) or confirmed AD (AD). n = 7 to 10 per group. **P < 0.01, Kruskal-Wallis analysis of variance (ANOVA), followed by Dunn's multiple-comparison test. (**G**) Representative Western blots from the superior frontal gyrus of controls (C), early-stage AD patients (E), and confirmed AD patients (A) for p-c-Jun, total c-Jun, p-JNK, CP13, PHF1, Tau13, and glyceraldehyde-3-phosphate dehydrogenase (GAPDH) (CP13 and PHF1 antibodies recognize hyperphosphorylated Tau). Asterisk symbol (*) represents an AD patient that was excluded from analysis because of the absence of Tau pathology. (**H**) Quantification of p-c-Jun and p-JNK, each normalized to GAPDH. **P < 0.01, ANOVA, followed by Dunnett's test. (**I**) Correlation between the amount of p-c-Jun and p-JNK with PHF1. *P < 0.05 and **P < 0.01, linear regression analysis. Open circles, controls; triangles, early-stage AD; filled circles, confirmed AD.

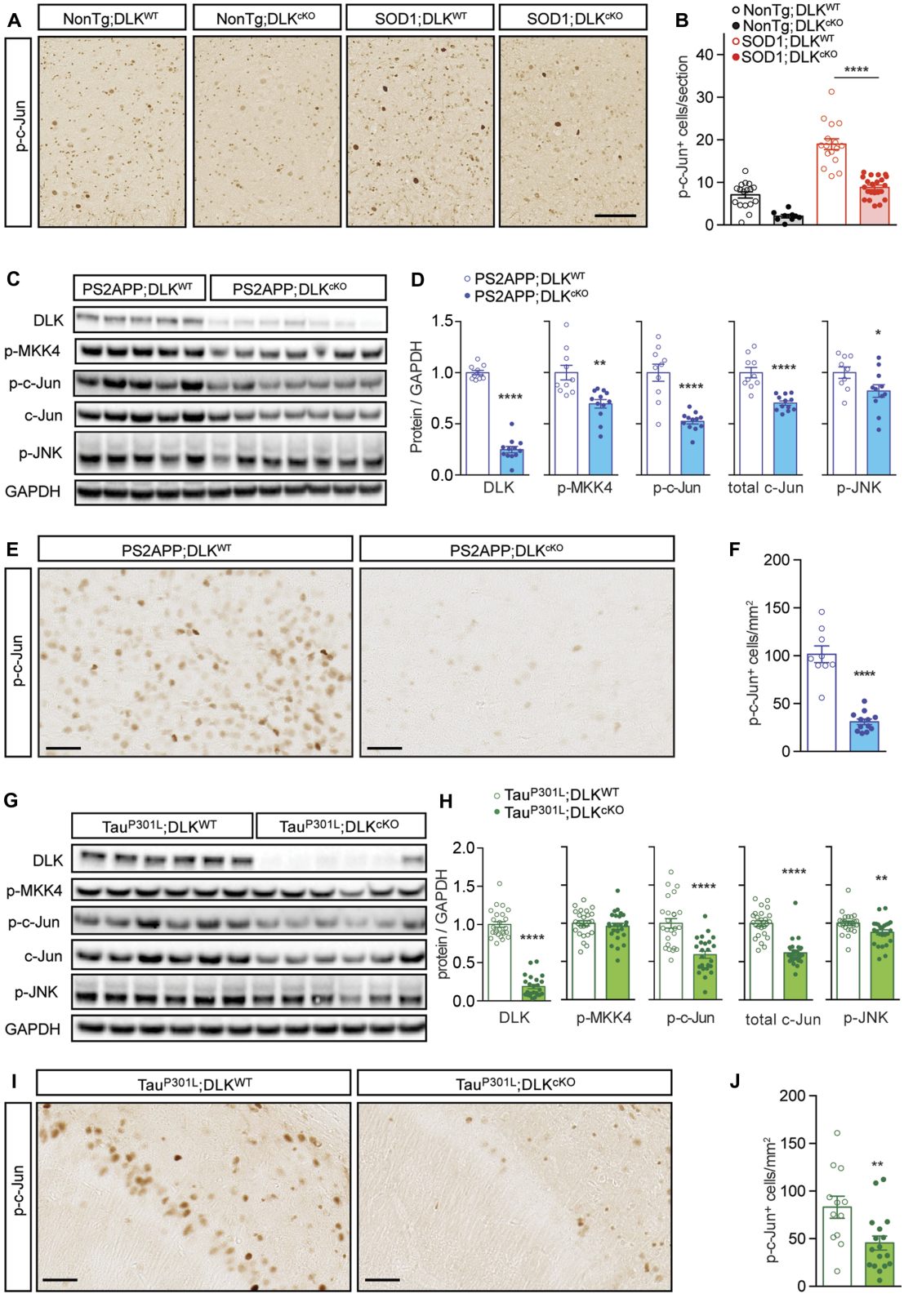

Fig. 3. *Dlk* deletion reduces p-c-Jun in AD and ALS mouse models. (**A**) Representative staining for p-c-Jun in spinal cord ventral horn of$SOD1^{G93A}$;DLK^{cKO} mice and nonTg controls. Scale bar, 100 μm. (**B**) p-c-Jun–positive cells per section in mouse L3 to L5 lumbar spinal cord by genotype. Each point represents the average value for one animal: 17 nonTg;DLK^{WT}, 9 nonTg;DLK^{cKO}, 16 $SOD1^{G93A}$;DLK^{WT}, and 22 $SOD1^{G93A}$;DLK^{cKO}. *P* values were determined by Tukey's post hoc pairwise comparisons after ANOVA with significance for $SOD1^{G93A}$ genotype ($F_{1,60}$ = 110.5, $P < 0.0001$), DLK genotype ($F_{1,60}$ = 72.3, $P < 0.0001$), and an interaction ($F_{1,60}$ = 8.3, $P = 0.0055$). (**C**) Western blot for DLK, p-MKK4, p-c-Jun, total c-Jun, and p-JNK in cortical lysates of 9-month-old PS2APP;DLK^{cKO} and PS2APP;DLK^{WT} mice. (**D**) Quantification of all markers in (C) from PS2APP;DLK^{cKO} (n = 10) versus PS2APP;DLK^{WT} (n = 12) mice. *$P < 0.05$, **$P < 0.01$, and ****$P < 0.0001$, two-tailed Student's t test. (**E**) Representative p-c-Jun immunostaining in ventral hippocampus of PS2APP;DLK^{cKO} and PS2APP;DLK^{WT} mice. Scale bars, 40 μm. (**F**) Quantification of p-c-Jun–positive cells per square millimeter tissue in PS2APP;DLK^{cKO} (n = 9) compared to PS2APP;DLK^{WT} (n = 12) mice. (**G**) Western blot of DLK, p-MKK4, p-c-Jun, total c-Jun, and p-JNK in cortical lysates of 9-month-old Tau^{P301L};DLK^{cKO} and Tau^{P301L};DLK^{WT} mice. (**H**) Quantification of all markers in (G) from Tau^{P301L};DLK^{cKO} (n = 24) compared to Tau^{P301L};DLK^{WT} mice (n = 25). **$P < 0.01$ and ****$P < 0.0001$, two-tailed Student's t test. (**I**) Representative p-c-Jun immunostaining in dorsal hippocampus of Tau^{P301L};DLK^{cKO} and Tau^{P301L};DLK^{WT} mice. Scale bars, 40 μm. (**J**) Mean number of p-c-Jun–positive cells per square millimeter in Tau^{P301L};DLK^{cKO} (n = 17) compared to Tau^{P301L};DLK^{WT} mice (n = 14). *$P < 0.05$, **$P < 0.01$, and ****$P < 0.0001$, two-tailed Student's t test (F and I).

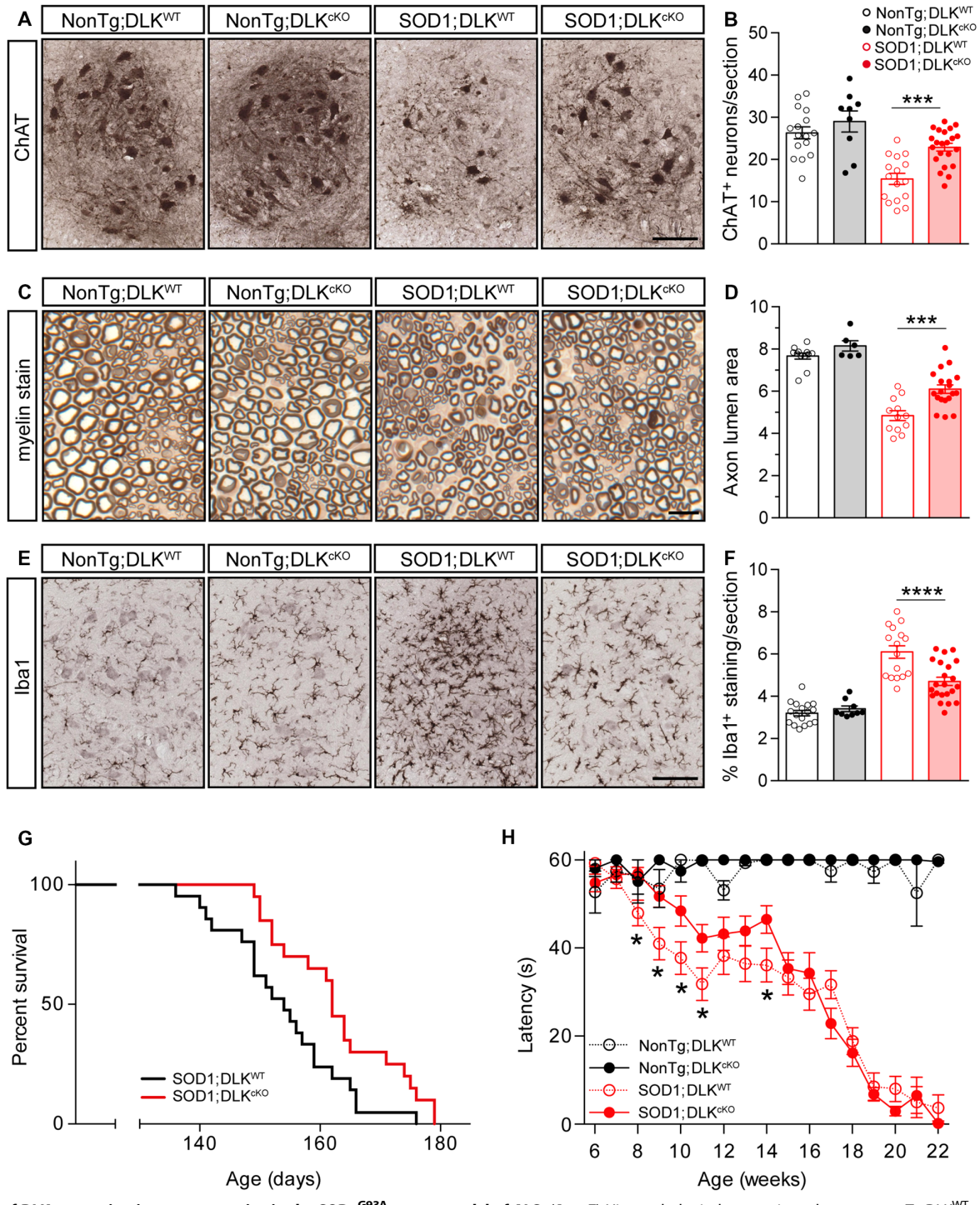

Fig. 4. Loss of DLK expression is neuroprotective in the SOD1^{G93A} mouse model of ALS. (**A** to **F**) Histopathological comparisons between nonTg;DLK^{WT}, nonTg;DLK^{cKO}, SOD1^{G93A};DLK^{cKO}, and SOD1^{G93A};DLK^{WT} littermates at 14 weeks of age. (A) Representative ChAT-positive staining in mouse spinal cord ventral horn. (B) Quantification of ChAT-positive neurons. ***$P < 0.001$, Tukey's test between SOD1^{G93A};DLK^{cKO} and SOD1^{G93A};DLK^{WT} mice. (C) Representative image of myelin staining in cross sections of mouse sciatic nerve. (D) Quantification of axonal lumen area. ***$P < 0.001$. (E) Iba1 immunostaining in mouse spinal cord ventral horn. (F) Quantification of Iba1-positive microglia. ****$P < 0.0001$, Tukey's test between SOD1^{G93A};DLK^{cKO} and SOD1^{G93A};DLK^{WT}. Each data point in (B), (D), and (F) represents the average value for one animal in a cohort of nonTg;DLK^{WT} ($n = 16$), nonTg;DLK^{cKO} ($n = 9$), SOD1^{G93A};DLK^{WT} ($n = 16$), and SOD1^{G93A};DLK^{cKO} ($n = 22$) mice. Scale bars, 100 μm (A and E) and 10 μm (C). (**G**) Kaplan-Meier curves showing survival of SOD1^{G93A};DLK^{cKO} versus SOD1^{G93A};DLK^{WT} littermates (median, 162 versus 154 days): SOD1^{G93A};DLK^{cKO} (red), $n = 23$ (with three being censored because of non-ALS death and not represented in graph); SOD1^{G93A};DLK^{WT} (black), $n = 21$ (with none being censored). Log-rank test (*$P = 0.0085$) for the whole model, with a significant DLK genotype effect (**$P = 0.0028$); sex effect (not significant). (**H**) Latency to fall on the wire hang test in SOD1^{G93A};DLK^{cKO} mice compared to SOD1^{G93A};DLK^{WT} littermates. Repeated-measures ANOVA from 6 to 14 weeks: Significant effects for DLK genotype ($P = 0.0062$), SOD1^{G93A} genotype ($P < 0.0001$), and sex ($P = 0.0045$); interaction of SOD1^{G93A} genotype × sex (not significant). *$P < 0.05$, Student's t test for individual time points comparing SOD1^{G93A};DLK^{WT} andSOD1^{G93A};DLK^{cKO}.

To determine whether the protection of motor neurons after *Dlk* deletion would provide lasting functional benefit, we examined symptom progression and life span in an independent cohort of $SOD1^{G93A}$;DLK^{cKO} mice. We found that loss of DLK increased the median life span of $SOD1^{G93A}$;DLK^{cKO} mice by 8 days compared to $SOD1^{G93A}$ mice expressing wild-type DLK (Fig. 4G) while controlling for $SOD1^{G93A}$ transgene copy number (fig. S4B) (*33*). Furthermore, $SOD1^{G93A}$;DLK^{cKO} mice displayed improvements in functional outcomes (fig. S3, E and F) (*34*), including the wire hang test, a measure of motor strength (Fig. 4H and fig. S3G). *Dlk* deletion was well tolerated, with only minor reductions in body weights (fig. S3, H and I).

Dlk deletion is beneficial in two mouse models of AD

In AD, reductions in dendritic spine densities are greatest within close proximity to amyloid plaques (*35*), which can be recapitulated in mouse models (*24*, *36*–*39*). On the basis of previous work, this end point can serve as an indicator of synaptic loss and provides a valuable measure of degenerative processes because neuronal loss is not a common feature of amyloid precursor protein (APP) transgenic mouse models of AD (*40*, *41*). Because DLK is present in the postsynaptic density and mediates neuronal degeneration after excitotoxic injury (*4*), we sought to determine whether plaque-associated synaptic loss is DLK-dependent through measurement of synaptic spine densities after selective deletion of *Dlk* from individual layer II/III neurons (*4*). Ex vivo imaging found 30% less spine loss proximal to plaques in PS2APP;DLK null neurons compared with PS2APP;DLK wild-type neurons (Fig. 5, A and B), indicating that Aβ/plaque-associated synaptic loss is at least in part mediated by DLK signaling.

Because loss of synaptic spines is associated with cognitive decline both in human AD patients and in some animal models of AD (*24*, *36*–*39*, *42*, *43*), we next compared cognitive function in >7-month-old PS2APP mice, in which *Dlk* deletion was induced at 10 to 12 weeks of age. PS2APP mice with intact DLK showed impairment in acquisition of active avoidance behavior (Fig. 5C) (*24*, *36*). However, loss of DLK expression resulted in a complete rescue of the PS2APP phenotype, with the PS2APP;DLK^{cKO} mice performing equally as well as nonTg controls on this task (Fig. 5C; $P < 0.001$). Spatial learning and memory were assessed in the Morris water maze, but no significant PS2APP transgene–dependent differences were found in this cohort of mice such that assessment of DLK function was not possible (fig. S5A). Fear-conditioning acquisition and 24-hour context fear memory were also not significantly different in PS2APP mice compared to nonTg controls (fig. S5, C to F). However, an increased freezing response to an audible tone (cued memory) was detected in PS2APP;DLK^{WT} animals, which was rescued in PS2APP;DLK^{cKO} mice (fig. S5, G and H). These results demonstrate that deletion of *Dlk* in young mice results in rescue of certain behavioral phenotypes in PS2APP mice. To determine whether DLK removal would have similar benefits after initiation of Aβ/plaque deposition and associated JNK/DLK pathway activation, we deleted *Dlk* at 6 months of age in an independent cohort of PS2APP;DLK^{cKO} mice (fig. S6A). These mice showed improvement in the active avoidance learning test (Fig. 5D; $P < 0.01$), suggesting that loss of DLK even subsequent to activation of the DLK/JNK pathway may be sufficient to reverse cognitive deficits in this task.

We next examined whether loss of DLK resulted in altered Aβ/plaque pathology in the PS2APP mice. Although synaptic spine density and cognitive function were improved after *Dlk* deletion, Aβ42 production and plaque load were not reduced (fig. S6). At older ages, PS2APP;DLK^{cKO} mice had slightly higher levels of full-length APP, amyloid plaques, and plaque-associated gliosis (fig. S6, B to K). These increases were not a result of altered β-secretase 1 (BACE1) (fig. S6, E and F) but could be explained by an aberrant up-regulation of *hAPP* expression driven by the Thy1 (thymus cell antigen 1) promoter (fig. S6, E to G). This observation was consistent with the previous finding that stress-induced Thy1 down-regulation is prevented in DLK^{cKO} mice (*5*), suggesting that the increase in plaque pathology was specific to this mouse model. *APP* expression changes in the PS2APP;DLK^{cKO} mice were specific to the Thy1-driven *hAPP* gene, whereas *mAPP* and prion protein (PrP) promoter–driven expression of *hPS2* were unaffected (fig. S6, E to G).

To provide a second measure of AD-related neurodegeneration in a model that displays more robust cell loss, we also assessed DLK function in Tau^{P301L} mice. The amount of total and phosphorylated Tau (p-Tau) was unchanged at 15 months of age (fig. S7, A and B), suggesting that loss of DLK did not alter Tau pathology. We found a significant attenuation of cell loss in the subiculum of Tau^{P301L};DLK^{cKO} mice (Fig. 5, E and F; $P < 0.05$), a brain area that develops Tau pathology (*44*). Collectively, the results from these three independent models of chronic neurodegenerative disease demonstrate that *Dlk* deletion, even after disease onset, results in increased neuronal survival, enhanced synaptic integrity, and some functional benefits.

Treatment with DLK inhibitors is neuroprotective and can reverse injury-induced changes in gene expression

Before examining the activity of two structurally distinct DLK inhibitors, GNE-8505 (fig. S8) and GNE-3511 (*15*), in chronic neurodegenerative disease mouse models, we first sought to better characterize the in vivo activity of these compounds using an acute optic nerve crush model where genetic deletion of *Dlk* or DLK inhibition before crush injury reduced injury-induced phosphorylation of c-Jun (*15*, *16*). To determine whether DLK inhibitors reduced p-c-Jun when administered after injury, we gave the animals a single dose of GNE-8505 18 hours after optic nerve crush, and we measured the amount of p-c-Jun in mouse retina at several time points. A single oral dose of GNE-8505 rapidly reduced p-c-Jun in a dose-dependent fashion within 1 hour, a decrease that was sustained for at least 6 hours (Fig. 6A). p-c-Jun repression correlated with the plasma concentration of GNE-8505, allowing all time points to be pooled to generate an in vivo dose-response curve (Fig. 6B). The calculated in vivo half maximal inhibitory concentration (IC_{50}) value of 0.98 ± 0.11 μM was consistent with the cellular IC_{50} for this compound when corrected for protein binding (table S2) and suggested that continuous DLK activity was required to maintain c-Jun phosphorylation (and, conversely, that repressing p-c-Jun would require sustained DLK inhibition).

Previous microarray studies in DLK^{cKO} mice revealed that DLK signaling not only regulates c-Jun phosphorylation but is also required for most of the injury-induced transcriptional changes after optic nerve crush (*5*). To determine whether DLK inhibition has the same effect, we gave the animals two doses of GNE-3511, starting at 3 days after nerve crush, and we assessed DLK-dependent gene expression by RNA sequencing (RNA-seq). As observed in previous studies (*5*), optic nerve injury induced numerous gene expression changes in vehicle-treated animals 3 days after injury. Just 12 hours of GNE-3511 treatment was sufficient to attenuate many of the injury-induced gene expression changes, with 148 up-regulated and 105 down-regulated genes demonstrating DLK dependence (Fig. 6C; $P < 0.05$). The DLK dependence of eight representative stress-induced genes, including Sprr1a, Atf3, Ddit3, and Bbc3, was then confirmed in a distinct cohort of animals (fig. S9).

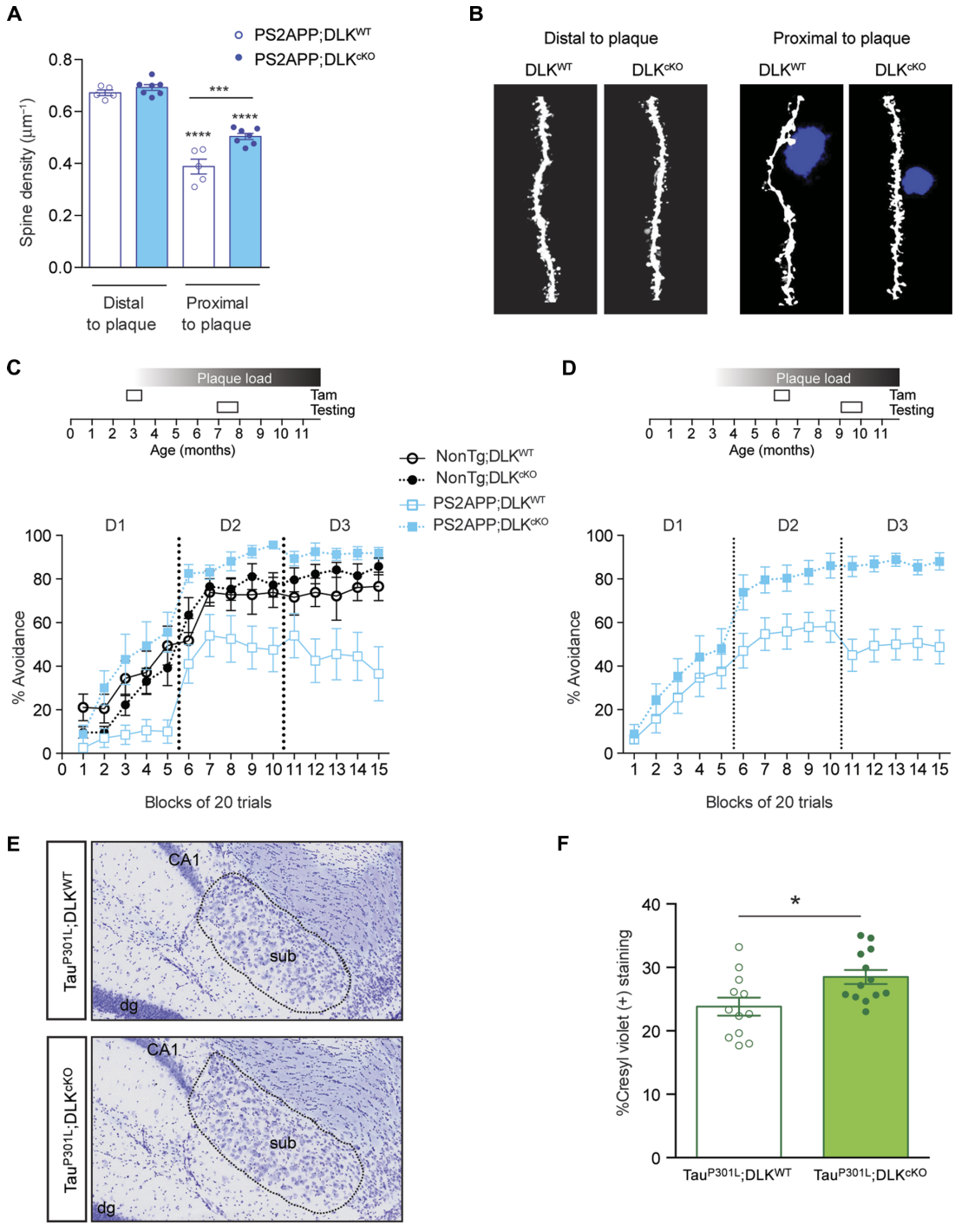

Fig. 5. Loss of DLK expression is neuroprotective in the PS2APP mouse model of AD. (**A**) Ex vivo imaging of spine densities (per micrometer) proximal to plaques (<100 µm) in layer II/III neurons of the somatosensory cortex of PS2APP;DLK^{lox};Cre^{pos} (DLK^{cKO}, $n = 7$) compared to PS2APP;DLK^{lox};Cre^{neg} (DLK^{WT}, $n = 5$) mice. Two-way ANOVA: Significant effects for DLK genotype ($F_{1,10} = 14.0$, $P < 0.01$), plaque location ($F_{1,10} = 311.5$, $P < 0.0001$), and an interaction ($F_{1,10} = 12.76$, $P < 0.01$). ****$P < 0.0001$ versus distal to plaque and ***$P < 0.001$ PS2APP;DLK^{cKO} versus PS2APP;DLK^{WT}, Sidak's post hoc test. (**B**) Representative images of dendritic spines distal (left) and proximal (right) to plaques (blue) stained with Methoxy-X04. (**C**) Deletion of DLK at 10 weeks of age induced by tamoxifen (Tam) improved active avoidance learning in PS2APP mice when trained at 7 to 8 months of age. Percentage of active avoidance responses during behavioral training revealed an overall DLK effect ($F_{1,36} = 13.2$, $P < 0.001$) and DLK × block interaction ($F_{1,36} = 11.3$, $P < 0.01$) over the 3 days of training by two-way repeated-measures ANOVA. PS2APP;DLK^{cKO} mice performed significantly better than PS2APP;DLK^{WT} mice ($F_{1,16} = 20.2$, $P < 0.001$, two-way repeated-measures ANOVA) for 9 nonTg;DLK^{WT}, 13 nonTg;DLK^{cKO}, 10 PS2APP;DLK^{WT}, and 8 PS2APP;DLK^{cKO} mice. (**D**) PS2APP;DLK^{cKO} mice ($n = 13$) in which DLK was deleted at 6 months of age performed significantly better in an active avoidance task than did PS2APP;DLK^{WT} mice ($n = 17$) when trained at 9 to 10 months of age. Two-way repeated-measures ANOVA found a significant effect of DLK^{cKO} ($F_{1,28} = 9.06$, $P < 0.01$) and a DLK^{cKO} × block interaction ($F_{14,392} = 4.42$, $P < 0.0001$). (**E**) Representative images of cresyl violet staining in the subiculum of the hippocampus in 15-month-old Tau^{P301L} transgenic mice. (**F**) Quantification of subicular cell loss in Tau^{P301L};DLK^{WT} mice ($n = 12$) compared to Tau^{P301L};DLK^{cKO} mice ($n = 13$). *$P = 0.0163$, two-tailed Student's t test.

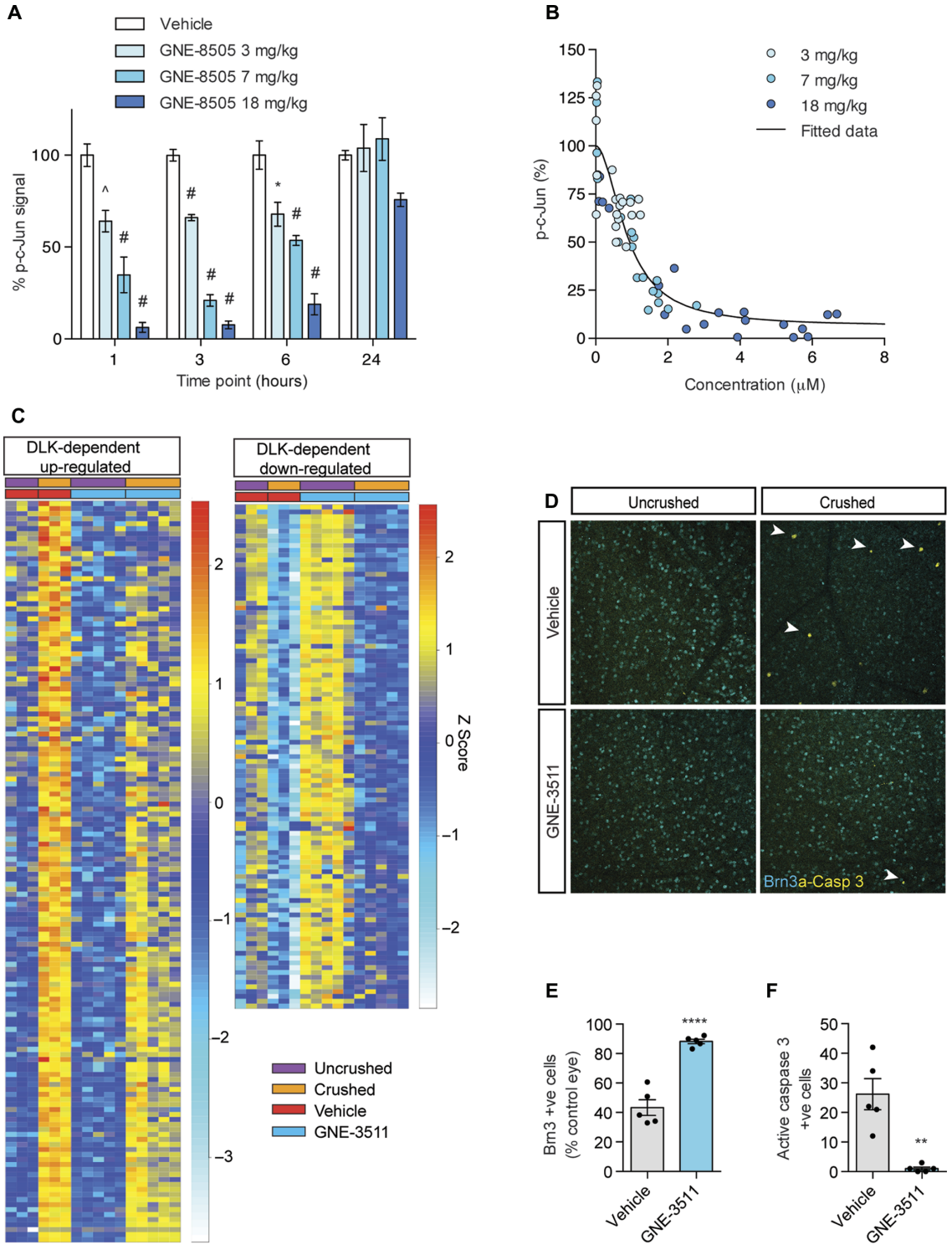

Fig. 6. Treatment with a DLK inhibitor is neuroprotective and reverses stress-induced gene expression changes. (**A**) The amount of p-c-Jun measured by enzyme-linked immunosorbent assay in retinal lysates after optic nerve crush in wild-type C57BL/6J mice dosed with vehicle or GNE-8505 at 3, 7, or 18 mg/kg ($n = 8$ per group). Data are normalized to vehicle-treated samples for each time point. Symbols denote significant differences compared with the vehicle group for each time point. $^{*}P < 0.05$, $^{\wedge}P < 0.001$, $^{\#}P \leq 0.0001$, Dunnett's test. (**B**) The pharmacokinetic/pharmacodynamic relationship between total drug exposure and reductions in p-c-Jun measured in (A) was used to calculate an in vivo IC_{50} of 0.983 ± 0.106 μM (mean ± SEM). (**C**) Heat map of injury-induced gene expression changes in mouse retinas 72 hours after optic nerve crush injury measured by RNA-seq for vehicle-treated or GNE-3511–treated mice (75 mg/kg; dosed 60 and 68 hours after crush). Comparison of injury-induced genes that are differentially regulated by GNE-3511 (1.2-fold, $P < 0.05$) identified 148 up-regulated and 105 down-regulated genes. (**D**) Representative staining of Brn3-positive (cyan) and activated caspase 3–positive (yellow) neurons in flat-mounted retinal samples (white arrowheads). (**E** and **F**) Quantification of Brn3-positive neurons [$^{****}P < 0.0001$, two-tailed Student's *t* test (E)] and active caspase 3–positive neurons [$^{**}P < 0.01$, two-tailed Student's *t* test (F)] in mouse retinas after optic nerve crush with or without GNE-3511 treatment.

To determine whether the reversal of injury-induced DLK signaling was sufficient to elicit neuroprotection in the mouse retina, we administered GNE-3511 twice daily for 3 days starting at 18 hours after optic nerve crush. Treatment with DLK inhibitors resulted in a significant reduction in retinal ganglion cell (RGC) apoptosis (by 96%; $P = 0.0014$) and maintenance of Brn3 expression (by 50%; $P < 0.0001$) in RGCs 3 days after crush injury (Fig. 6, D to F). This demonstrated that inhibition of DLK resulted in neuroprotection similar to that seen in DLK^{cKO} animals even when dosing was initiated after injury (*5*).

DLK inhibition is beneficial in a mouse model of ALS

We next sought to determine whether pharmacological inhibition of DLK could have beneficial effects in a chronic neurodegenerative disease mouse model. These studies focused largely on the $SOD1^{G93A}$ transgenic mouse model of ALS where degeneration of motor neurons and loss of neuromuscular junctions are characteristic of the disease and can be readily monitored. We first tested whether short-term DLK inhibition was sufficient to reverse existing DLK/JNK signaling in vivo. GNE-3511 treatment reduced the number of p-c-Jun–positive cells in a dose-dependent manner in the spinal cords of 14-week-old $SOD1^{G93A}$ mice when compared with vehicle-treated animals (Fig. 7, A to C). Similar results were obtained with GNE-8505 treatment (Fig. 7B), confirming that this effect was a result of DLK inhibition. Furthermore, a single dose of GNE-8505 was sufficient to elicit a comparable dose-dependent reduction in brain p-c-Jun at 6 hours after dose in both PS2APP and Tau^{P301L} mice, suggesting that this observation was not specific to the $SOD1^{G93A}$ mouse model (fig. S10). Thus, acute treatment of mid–disease stage animals with DLK inhibitors reduced activity in the DLK/JNK signaling pathway and decreased p-c-Jun even when disease-related JNK signaling had been present for weeks before drug treatment.

To determine whether DLK inhibitor treatment was able to protect motor neurons from degeneration, we first treated cultured mouse embryonic stem cell–derived HB9-GFP (HB9–green fluorescent protein)–positive motor neurons with GNE-3511 after trophic factor withdrawal. A dose-dependent increase in motor neuron survival was observed at 24 hours after addition of the compound (Fig. 7, D and E). We then examined whether chronic GNE-3511 treatment was able to slow disease progression in $SOD1^{G93A}$ mice. In an effort to design a feasible preclinical study in which the $SOD1^{G93A}$ mice were receiving adequate dosing while minimizing dosing-related stress, we opted to administer GNE-3511 in food and assessed an early measure of disease progression, neuromuscular junction loss. Loss of innervation of the neuromuscular junctions in gastrocnemius muscle is one of the first signs of disease in this model (*45*, *46*), with more than 50% of neuromuscular junctions showing complete denervation by 9 weeks of age. Notably, GNE-3511 treatment delayed neuromuscular junction denervation by ~10% (Fig. 7, F to H, and fig. S11; $P = 0.0094$) compared to vehicle-treated $SOD1^{G93A}$ mice, demonstrating that chronic inhibition of DLK between 5 and 9 weeks of age was able to provide neuroprotection in this mouse model of ALS.

DISCUSSION

Here, we demonstrate that either genetic deletion or pharmacological inhibition of DLK is sufficient to reduce disease-associated JNK pathway activation and provide functional neuroprotection in mouse models of ALS and AD. The function of DLK signaling described here is consistent with reports examining DLK function after acute insults, such as axonal injury, excitotoxic insult, and MPTP (1-methyl-4-phenyl-1,2,3,6-tetrahydropyridine) treatment (*3*–*5*, *15*, *47*), suggesting that DLK represents a conserved component of the neuronal stress response that is downstream of a variety of insults. This, along with the observation that similar JNK pathway activation exists in the CNS of patients with ALS and AD, supports the hypothesis that DLK signaling contributes to neuronal degeneration and subsequent functional decline in a range of neurodegenerative diseases.

The number of p-c-Jun–positive neurons present in the $SOD1^{G93A}$ mouse model of ALS was considerably higher than the number expected to be undergoing apoptosis at any given time (*18*). In addition, widespread p-c-Jun–positive cells are present in PS2APP mice, although extensive neuronal loss does not occur in this AD mouse model (*40*, *41*). These observations suggest that DLK activation may not lead directly to apoptosis. Instead, neurons appear to undergo an extended period of stress, suggesting that DLK/JNK signaling may also contribute to degeneration of neuronal processes and synapse loss. The rescue of synaptic spines in PS2APP mice via *Dlk* deletion provides a direct demonstration that loss of this prodegenerative signal protects against subapoptotic cellular damage. Last, the cognitive improvements observed in PS2APP mice after late *Dlk* deletion argues that meaningful functional benefit can be achieved by halting existing neuronal DLK/JNK signaling. These observations along with the rapid reversal of c-Jun phosphorylation and stress-induced transcriptional changes within hours of a single DLK inhibitor treatment argue that individual neurons can still be rescued from degeneration after DLK/JNK pathway activation. Data from multiple studies indicate that some adaptive/proregenerative stress responses may also take place in p-c-Jun–positive neurons (*5*, *9*–*12*), yet the functional benefits observed in DLK^{cKO} animals argue that loss of DLK signaling provides a net benefit in the context of chronic neurodegeneration.

Nonetheless, important questions must still be answered to accurately assess the therapeutic potential of this approach. First, although the histological protection of neurons in DLK^{cKO} mice was robust across models, it is challenging to determine whether the effect size observed in the functional end points measured would be likely to translate to clinical benefit. Second, additional studies are needed to determine the level of DLK inhibition required to maintain efficacy after chronic drug treatment and to confirm that these doses will be tolerated. Although encouraging progress has been made toward the development of selective brain-penetrant DLK inhibitors (*15*, *16*), it has historically proved challenging to design kinase inhibitors that are well tolerated in clinical studies.

There are a number of considerations, however, that make targeting DLK more attractive than other approaches aimed at inhibition of JNK signaling. First, DLK expression is enriched in neurons and specifically regulates stress-induced JNK signaling (*32*, *48*, *49*), providing a specific means to target neuronal dysfunction in CNS disease, in contrast to many other components of the JNK signaling pathway (*32*). Second, loss of DLK signaling in the adult is well tolerated (*4*). Third, given the broad regulation of the transcriptional stress response in neurons via DLK signaling and the ability of DLK inhibitors to rapidly reverse injury-induced gene expression changes (Fig. 6), DLK inhibitor treatment could potentially attenuate a range of downstream signaling events in the context of progressive degeneration (*5*). Given the consistent role for DLK/JNK signaling in multiple disease models driven by diverse mechanisms, DLK inhibitors hold broad therapeutic potential and may warrant advancement to clinical studies should safe compounds be identified.

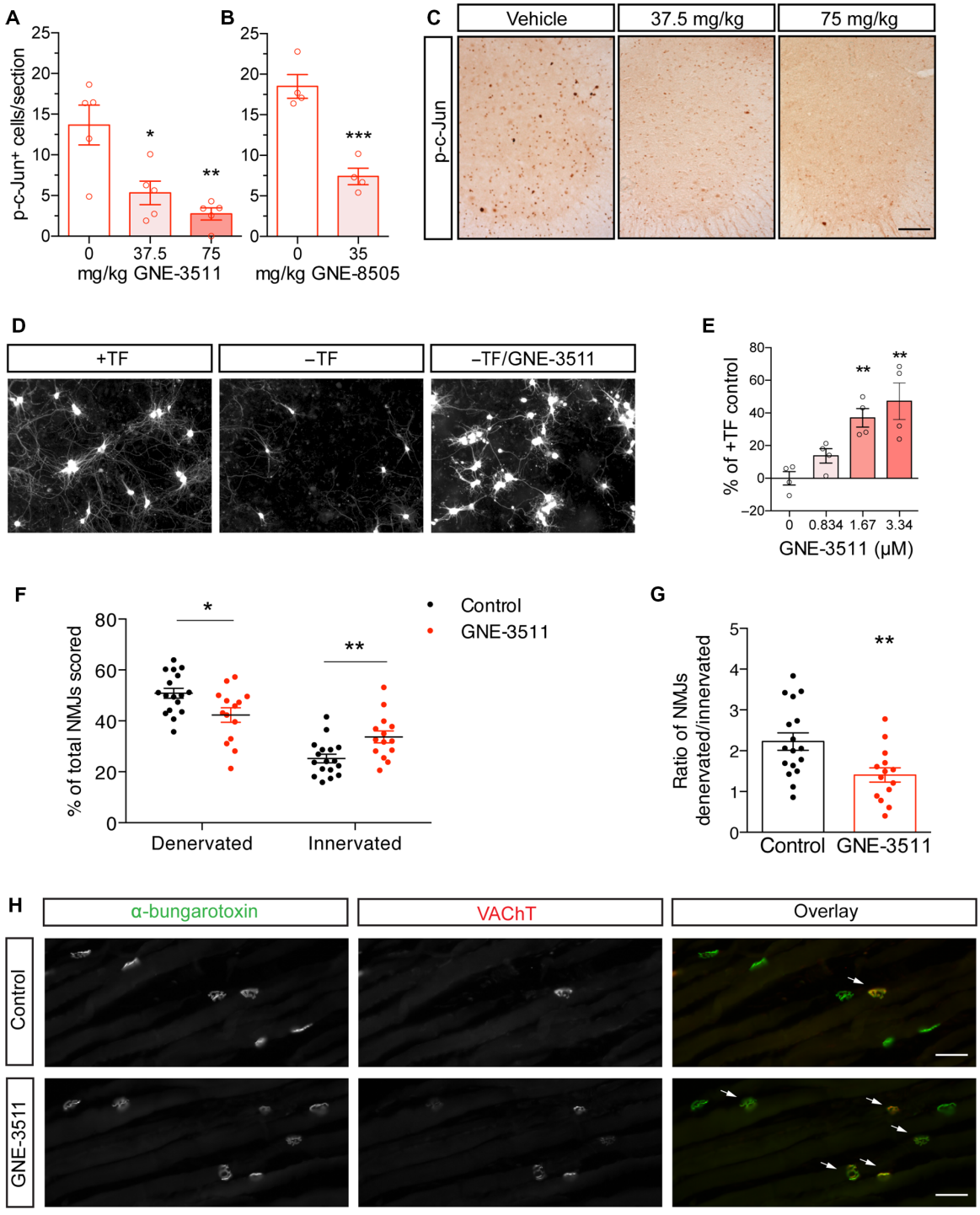

Fig. 7. Treatment with DLK inhibitors reduces p-c-Jun and protects against neuronal and synaptic loss in vitro and in ALS mouse models. (**A**) Quantification of p-c-Jun–positive cells/spinal cord section in SOD1^{G93A} mice after treatment with vehicle (0 mg/kg) or GNE-3511 (37.5 or 75 mg/kg) (n = 5 per group). ANOVA: Significant treatment effect ($F_{2,12}$ = 11.3, P < 0.0017). *P < 0.05 and **P < 0.01,Tukey's test, versus vehicle (0 mg/kg). (**B**) Quantification of p-c-Jun–positive cells per section after treatment with vehicle (0 mg/kg) or GNE-8505 (35 mg/kg) (n = 4 per group; ***P < 0.001). (**C**) Representative images of each dose group shown in (A). Scale bar, 100 μm. (**D**) Representative images of HB9-GFP–positive motor neurons in the presence (+TF) or absence (−TF) of trophic factors or without trophic factors plus 3.34 μM GNE-3511. (**E**) Quantification of GFP-positive neurite area for trophic factor–deprived motor neurons exposed to increasing concentrations of GNE-3511. ANOVA: Significant treatment effect ($F_{3,12}$ = 9.529, P < 0.01). **P < 0.01, Dunnett's test, versus vehicle (0 mg/kg) dose group. (**F**) Quantification of α-bungarotoxin–positive neuromuscular junctions (NMJs) that were either denervated or fully innervated [as measured by proximity to vesicular acetylcholine transporter (VAChT)–positive pixels] in GNE-3511–treated (n = 14) versus vehicle-treated (n = 17) SOD1^{G93A}mice. *P = 0.0289 and **P = 0.0094 versus control littermates. (**G**) Ratio of denervated to innervated neuromuscular junctions is decreased in GNE-3511–treated SOD1^{G93A}mice. **P < 0.01. (**H**) Representative images of neuromuscular junction synapses from vehicle- and GNE-3511–treated SOD1^{G93A} mice. Red, presynaptic side (VAChT); green, postsynaptic side (α-bungarotoxin). White arrows indicate innervated synapses. Scale bars, 50 μm.

MATERIALS AND METHODS

Study design

The primary research objectives of this study were to assess whether mouse models of neurodegeneration (including SOD1^{G93A}, PS2APP, and Tau^{P301L} mice) and CNS tissue from patients with ALS and AD display evidence of increased DLK pathway activity and to test whether genetic deletion or pharmacological inhibition of DLK could ameliorate end points of disease progression. In all experiments, animals were randomly assigned to experimental or treatment groups and matched for age, sex, and littermate controls. All behavioral scorings and histological analyses were carried out blind to genotype and treatment groups. Any SOD1^{G93A} transgenic mouse with a reduced transgene copy number was excluded (fig. S4). All animal studies were authorized and approved by the Genentech Institutional Animal Care and Use Committee. Human samples were procured with Ethics Committee approval and written informed consent.

Mice

ALS mouse models used in this work were the SOD1^{G93A} high–copy number transgenic mice (SOD1) originally derived from the Jackson Laboratory [JAX stock #002726 (*21*)] and backcrossed for at least 10 generations into C57BL/6N (Charles River Laboratories) and TDP-43^{A315T} (JAX #010700) (*23*). Treatment groups for all experiments using SOD1 mice were balanced for gender and litter, and all mice were genotyped for SOD1 copy number (fig. S4 and table S1). AD mouse models used in this study included PS2APP mice that coexpress human APP (hAPP) with the Swedish mutation K670N/M671L and human presenilin 2 with the N141I mutation, driven by Thy1 and PrP promoters, respectively (*25*). Tau^{P301L} mice overexpress mutant human Tau with the P301L mutation (*26*) driven by the Thy1 promoter. The PS2APP and Tau alleles in each line were bred to homozygosity for all mice used in this study.

Inducible DLK knockout mice were described previously (*4*). Briefly, DLK^{lox} mice were crossed with CAG-CreERT mice (JAX #004453) to generate DLK^{lox};Cre^{pos} or DLK^{lox};Cre^{neg} mice. These mice were then crossed with the SOD1^{G93A}, PS2APP, and Tau^{P301L} mice generating, for example, SOD1^{G93A};DLK^{lox};Cre^{neg} and SOD1^{G93A};DLK^{lox};Cre^{pos} mice, which are referred to as SOD1^{G93A};DLK^{WT} and SOD1^{G93A};DLK^{cKO}, respectively, after recombination. *Dlk* excision was achieved by placing the mice on a tamoxifen-containing diet (about 40 mg/kg per day) for 3 weeks to induce Cre-mediated DNA recombination. This protocol was found to generate maximal recombination efficiency of the *Dlk* allele in the CNS while minimizing the loss of animals due to tamoxifen toxicity. All mice in this study were placed on this diet, including nonTg controls, where applicable. SOD1^{G93A} mice were placed on the diet at 28 days of age and PS2APP and Tau^{P301L} mice at 10 to 12 weeks of age or 6 months of age. While on medicated chow, all mice appeared healthy and active overall despite modest weight loss (up to 10 to 15%). All mice were returned to regular chow diet after the tamoxifen treatment.

Human postmortem samples for Western blotting and immunohistochemistry

Frozen spinal cord tissues were procured from patients with sporadic ALS and control subjects with no known neurodegenerative diseases. These cases were clinically and neuropathologically evaluated at the University of California, San Francisco. Additional human tissue specimens were provided by the Department of Veterans Affairs Repository. Human frozen brain samples were procured from patients with putative AD (early-stage AD) or confirmed AD along with age-matched controls from Folio Biosciences or Banner Sun Health Research Institute. All human tissues were collected with informed consents and institutional review board approvals.

Tissue harvest and preparation

SOD1 mice were anesthetized with 2.5% tribromoethanol (0.5 ml/25 g body weight) and transcardially exsanguinated with phosphate-buffered saline (PBS) followed by 4% paraformaldehyde (PFA) in PBS for fixation. Gastrocnemius muscles were collected and cryoprotected in 30% sucrose. Sciatic nerve was harvested 2 to 3 cm proximal to the branch point of the tibial, peroneal, and sural nerves and postfixed in 4% PFA overnight. Spinal cords were harvested as previously described and postfixed in 4% PFA overnight, then transferred to PBS, and shipped to NeuroScience Associates for histology.

At indicated time points, PS2APP and Tau^{P301L} on DLK^{WT} or DLK^{cKO} background animals were deeply anesthetized and PBS-perfused. After PBS perfusion, the brain was collected, and the left hippocampus and cortex were frozen and later homogenized for Western blotting (see Supplementary Materials and Methods). The right forebrain was drop-fixed in 4% PFA for 48-hour shaking at 4°C, then cryoprotected in 30% sucrose, and sectioned sagittally at 35 μm using a sliding microtome. Sections were preserved in cryoprotectant (30% glycerol, 30% ethylene glycol, and PBS) and stored at −20°C.

Immunohistochemical staining

Spinal cord histology and staining

Lumbar spinal cord segments were sectioned and sampled as previously described (*45*). They were multiply embedded into a gelatin matrix using MultiBrain Technology (NeuroScience Associates). Each MultiBrain block was sectioned coronally at 25 μm. A series of 33 sections equally spaced at 300-μm intervals throughout the entire lumbar spinal cord was used for staining. Spinal cord sections were stained as previously described (*45*). Immunohistochemical staining was performed using goat anti-ChAT (Millipore AB144P), rabbit anti-GFAP (Dako Z0334), rabbit anti-Iba1 (Wako 019-19741), rabbit anti–p-c-Jun (Ser^{63}) II (Cell Signaling #9261), and mouse anti-NeuN (clone A60, Millipore MAB377).

Brain histology and staining

Free-floating sections (35 μm thick) were rinsed in PBS then PBS with 0.1% Triton X (PBST), treated with 3% hydrogen peroxide in PBST, and blocked with 5% bovine serum albumin (BSA) in PBST before overnight incubation at 4°C, with primary antibody diluted in 1% BSA in PBST [anti-Iba1 (1:1000), anti-GFAP (1:1000), and anti–p-c-Jun (Ser^{63}) II (1:600)]. Binding was detected with biotin-conjugated secondary antibodies, followed by avidin–biotin–horseradish peroxidase (HRP) complex (details in VECTASTAIN Elite ABC kit; Vector Laboratories #PK6100), and developed with diaminobenzidine tetrahydrochloride.

For detection of p-c-Jun (Ser^{63}) in human AD and control tissue, immunohistochemistry was performed on 4-μm-thick formalin-fixed, paraffin-embedded tissue sections mounted on glass slides. Staining was performed on Dako Autostainer using Target Retrieval Solution (Dako) for antigen retrieval. Detection used goat anti-rabbit biotinylated secondary antibody (Vector Laboratories), followed by VECTASTAIN Elite ABC HRP kit (Vector Laboratories) and metal-enhanced diaminobenzidine visualization (Thermo Fisher Scientific). The sections were counterstained with hematoxylin, dehydrated, and coverslipped.

Statistical analysis

Statistical tests were performed using GraphPad Prism 6.0 software (GraphPad Software Inc.) or JMP 10.0.2 software (SAS Institute Inc.). All data are presented as means ± SEM, except when stated otherwise in the figure legends. Unless otherwise stated, for quantitative cell morphology (spine density), biochemical, and histological analysis, statistical significance was assessed by Student's *t* test for comparison between two samples or by one-way or two-way ANOVA with post hoc Tukey-Kramer honest significant difference test for comparison across multiple groups or Dunnett's test versus controls. Nonparametric tests included Mann-Whitney test or Kruskal-Wallis ANOVA followed by Dunn's multiple-comparison test. For behavioral data collected over multiple sessions or positions (that is, active avoidance), we used multifactor repeated-measures ANOVA with the between-subjects factor of genotype (PS2APP or DLK) and the within-subjects factor of sessions (sessions or trials). For survival analysis of the SOD1 mice, a log-rank test was assessed for the whole model, with examination of DLK genotype and sex effects.

SUPPLEMENTARY MATERIALS

www.sciencetranslationalmedicine.org/cgi/content/full/9/403/eaag0394/DC1

Materials and Methods

Fig. S1. p-c-Jun is expressed in ChAT-positive motor neurons of SOD1 mice, and *Dlk* is coexpressed with neuronal markers.

Fig. S2. Elevations in p-c-Jun and c-Jun are detected in mouse models of AD.

Fig. S3. *Dlk* deletion is neuroprotective by histological and behavioral measures in the SOD1 mouse model of ALS.

Fig. S4. SOD1 transgene copy number data for the histological and survival studies shown in Fig. 4 and fig. S3.

Fig. S5. PS2APP;DLK^{cKO} behavior in the water maze and fear conditioning.

Fig. S6. DLK deletion in PS2APP mice results in slight elevation of plaque-associated gliosis and hAPP expression without altering BACE1.

Fig. S7. DLK deletion in Tau^{P301L} mice does not alter total Tau or p-Tau species.

Fig. S8. Chemical structure, selectivity, and pharmacokinetics of GNE-8505.

Fig. S9. qPCR of optic nerve crush mouse retinas for genes selected on the basis of the RNA-seq results.

Fig. S10. Short-term treatment with DLK inhibitors reduces p-c-Jun and total c-Jun levels in PS2APP and Tau^{P301L} mice.

Fig. S11. Classification of synaptic loss in the neuromuscular junction of SOD1 mice.

Table S1. Distribution of SOD1 mice in survival study according to euthanasia criteria.

Table S2. GNE-8505 inhibition constant in a DLK biochemical assay.

Reference (*50*)

REFERENCES AND NOTES

1. S. Vucic, J. D. Rothstein, M. C. Kiernan, Advances in treating amyotrophic lateral sclerosis: Insights from pathophysiological studies. *Trends Neurosci.* **37**, 433–442 (2014).
2. D. M. Holtzman, J. C. Morris, A. M. Goate, Alzheimer's disease: The challenge of the second century. *Sci. Transl. Med.* **3**, 77sr1 (2011).
3. A. Sengupta Ghosh, B. Wang, C. D. Pozniak, M. Chen, R. J. Watts, J. W. Lewcock, DLK induces developmental neuronal degeneration via selective regulation of proapoptotic JNK activity. *J. Cell Biol.* **194**, 751–764 (2011).
4. C. D. Pozniak, A. Sengupta Ghosh, A. Gogineni, J. E. Hanson, S.-H. Lee, J. L. Larson, H. Solanoy, D. Bustos, H. Li, H. Ngu, A. M. Jubb, G. Ayalon, J. Wu, K. Scearce-Levie, Q. Zhou, R. M. Weimer, D. S. Kirkpatrick, J. W. Lewcock, Dual leucine zipper kinase is required for excitotoxicity-induced neuronal degeneration. *J. Exp. Med.* **210**, 2553–2567 (2013).
5. T. A. Watkins, B. Wang, S. Huntwork-Rodriguez, J. Yang, Z. Jiang, J. Eastham-Anderson, Z. Modrusan, J. S. Kaminker, M. Tessier-Lavigne, J. W. Lewcock, DLK initiates a transcriptional program that couples apoptotic and regenerative responses to axonal injury. *Proc. Natl. Acad. Sci. U.S.A.* **110**, 4039–4044 (2013).
6. X. Chen, M. Rzhetskaya, T. Kareva, R. Bland, M. J. During, A. W. Tank, N. Kholodilov, R. E. Burke, Antiapoptotic and trophic effects of dominant-negative forms of dual leucine zipper kinase in dopamine neurons of the substantia nigra in vivo. *J. Neurosci.* **28**, 672–680 (2008).
7. B. R. Miller, C. Press, R. W. Daniels, Y. Sasaki, J. Milbrandt, A. DiAntonio, A dual leucine kinase-dependent axon self-destruction program promotes Wallerian degeneration. *Nat. Neurosci.* **12**, 387–389 (2009).
8. D. S. Welsbie, Z. Yang, Y. Ge, K. L. Mitchell, X. Zhou, S. E. Martin, C. A. Berlinicke, L. Hackler Jr., J. Fuller, J. Fu, L.-h. Cao, B. Han, D. Auld, T. Xue, S.-i. Hirai, L. Germain, C. Simard-Bisson, R. Blouin, J. V. Nguyen, C.-h. O. Davis, R. A. Enke, S. L. Boye, S. L. Merbs, N. Marsh-Armstrong, W. W. Hauswirth, A. DiAntonio, R. W. Nickells, J. Inglese, J. Hanes, K.-W. Yau, H. A. Quigley, D. J. Zack, Functional genomic screening identifies dual leucine zipper kinase as a key mediator of retinal ganglion cell death. *Proc. Natl. Acad. Sci. U.S.A.* **110**, 4045–4050 (2013).
9. M. Hammarlund, P. Nix, L. Hauth, E. M. Jorgensen, M. Bastiani, Axon regeneration requires a conserved MAP kinase pathway. *Science* **323**, 802–806 (2009).
10. J. E. Shin, Y. Cho, B. Beirowski, J. Milbrandt, V. Cavalli, A. DiAntonio, Dual leucine zipper kinase is required for retrograde injury signaling and axonal regeneration. *Neuron* **74**, 1015–1022 (2012).
11. X. Xiong, X. Wang, R. Ewanek, P. Bhat, A. Diantonio, C. A. Collins, Protein turnover of the Wallenda/DLK kinase regulates a retrograde response to axonal injury. *J. Cell Biol.* **191**, 211–223 (2010).
12. D. Yan, Z. Wu, A. D. Chisholm, Y. Jin, The DLK-1 kinase promotes mRNA stability and local translation in *C. elegans* synapses and axon regeneration. *Cell* **138**, 1005–1018 (2009).
13. A. M. Manning, R. J. Davis, Targeting JNK for therapeutic benefit: From junk to gold? *Nat. Rev. Drug Discov.* **2**, 554–565 (2003).
14. M. Gehringer, F. Muth, P. Koch, S. A. Laufer, c-Jun N-terminal kinase inhibitors: A patent review (2010–2014). *Expert Opin. Ther. Pat.* **25**, 849–872 (2015).
15. S. Patel, F. Cohen, B. J. Dean, K. De La Torre, G. Deshmukh, A. A. Estrada, A. Sengupta Ghosh, P. Gibbons, A. Gustafson, M. P. Huestis, C. E. Le Pichon, H. Lin, W. Liu, X. Liu, Y. Liu, C. Q. Ly, J. P. Lyssikatos, C. Ma, K. Scearce-Levie, Y. G. Shin, H. Solanoy, K. L. Stark, J. Wang, B. Wang, X. Zhao, J. W. Lewcock, M. Siu, Discovery of dual leucine zipper kinase (DLK, MAP3K12) inhibitors with activity in neurodegeneration models. *J. Med. Chem.* **58**, 401–418 (2015).
16. S. Patel, S. F. Harris, P. Gibbons, G. Deshmukh, A. Gustafson, T. Kellar, H. Lin, X. Liu, Y. Liu, Y. Liu, C. Ma, K. Scearce-Levie, A. Sengupta Ghosh, Y. G. Shin, H. Solanoy, J. Wang, B. Wang, J. Yin, M. Siu, J. W. Lewcock, Scaffold-hopping and structure-based discovery of potent, selective, and brain penetrant *N*-(1*H*-pyrazol-3-yl)pyridin-2-amine inhibitors of dual leucine zipper kinase (DLK, MAP3K12). *J. Med. Chem.* **58**, 8182–8199 (2015).
17. D. Jaarsma, J. C. Holstege, D. Troost, M. Davis, J. Kennis, E. D. Haasdijk, V. J. de Jong, Induction of c-Jun immunoreactivity in spinal cord and brainstem neurons in a transgenic mouse model for amyotrophic lateral sclerosis. *Neurosci. Lett.* **219**, 179–182 (1996).
18. A. S. Vlug, E. Teuling, E. D. Haasdijk, P. French, C. C. Hoogenraad, D. Jaarsma, ATF3 expression precedes death of spinal motoneurons in amyotrophic lateral sclerosis-SOD1 transgenic mice and correlates with c-Jun phosphorylation, CHOP expression, somato-dendritic ubiquitination and Golgi fragmentation. *Eur. J. Neurosci.* **22**, 1881–1894 (2005).
19. B. J. Pulverer, J. M. Kyriakis, J. Avruch, E. Nikolakaki, J. R. Woodgett, Phosphorylation of c-*jun* mediated by MAP kinases. *Nature* **353**, 670–674 (1991).
20. D. D. Yang, C.-Y. Kuan, A. J. Whitmarsh, M. Rincón, T. S. Zheng, R. J. Davis, P. Rakic, R. A. Flavell, Absence of excitotoxicity-induced apoptosis in the hippocampus of mice lacking the Jnk3 gene. *Nature* **389**, 865–870 (1997).
21. M. E. Gurney, H. Pu, A. Y. Chiu, M. C. Dal Canto, C. Y. Polchow, D. D. Alexander, J. Caliendo, A. Hentati, Y. W. Kwon, H. X. Deng, W. Chen, P. Zhai, R. L. Sufit, T. Siddique, Motor neuron degeneration in mice that express a human Cu,Zn superoxide dismutase mutation. *Science* **264**, 1772–1775 (1994).
22. K. C. Kanning, A. Kaplan, C. E. Henderson, Motor neuron diversity in development and disease. *Annu. Rev. Neurosci.* **33**, 409–440 (2010).
23. I. Wegorzewska, S. Bell, N. J. Cairns, T. M. Miller, R. H. Baloh, TDP-43 mutant transgenic mice develop features of ALS and frontotemporal lobar degeneration. *Proc. Natl. Acad. Sci. U.S.A.* **106**, 18809–18814 (2009).
24. D. Y. Kallop, W. J. Meilandt, A. Gogineni, C. Easley-Neal, T. Wu, A. M. Jubb, M. Yaylaoglu, M. Shamloo, M. Tessier-Lavigne, K. Scearce-Levie, R. M. Weimer, A death receptor 6-amyloid precursor protein pathway regulates synapse density in the mature CNS but does not contribute to Alzheimer's disease-related pathophysiology in murine models. *J. Neurosci.* **34**, 6425–6437 (2014).
25. L. Ozmen, A. Albientz, C. Czech, H. Jacobsen, Expression of transgenic APP mRNA is the key determinant for beta-amyloid deposition in PS2APP transgenic mice. *Neurodegener Dis* **6**, 29–36 (2009).
26. J. Götz, F. Chen, R. Barmettler, R. M. Nitsch, Tau filament formation in transgenic mice expressing P301L tau. *J. Biol. Chem.* **276**, 529–534 (2001).
27. A. G. Pearson, U. T. E. Byrne, G. A. MacGibbon, R. L. M. Faull, M. Dragunow, Activated c-Jun is present in neurofibrillary tangles in Alzheimer's disease brains. *Neurosci. Lett.* **398**, 246–250 (2006).
28. A. Thakur, X. Wang, S. L. Siedlak, G. Perry, M. A. Smith, X. Zhu, c-Jun phosphorylation in Alzheimer disease. *J. Neurosci. Res.* **85**, 1668–1673 (2007).
29. H. Braak, E. Braak, J. Bohl, Staging of Alzheimer-related cortical destruction. *Eur. Neurol.* **33**, 403–408 (1993).

30. E. T. Coffey, G. Smiciene, V. Hongisto, J. Cao, S. Brecht, T. Herdegen, M. J. Courtney, c-Jun N-terminal protein kinase (JNK) 2/3 is specifically activated by stress, mediating c-Jun activation, in the presence of constitutive JNK1 activity in cerebellar neurons. *J. Neurosci.* **22**, 4335–4345 (2002).
31. J. Kong, Z. Xu, Massive mitochondrial degeneration in motor neurons triggers the onset of amyotrophic lateral sclerosis in mice expressing a mutant SOD1. *J. Neurosci.* **18**, 3241–3250 (1998).
32. Y. Zhang, K. Chen, S. A. Sloan, M. L. Bennett, A. R. Scholze, S. O'Keeffe, H. P. Phatnani, P. Guarnieri, C. Caneda, N. Ruderisch, S. Deng, S. A. Liddelow, C. Zhang, R. Daneman, T. Maniatis, B. A. Barres, J. Q. Wu, An RNA-sequencing transcriptome and splicing database of glia, neurons, and vascular cells of the cerebral cortex. *J. Neurosci.* **34**, 11929–11947 (2014).
33. S. Scott, J. E. Kranz, J. Cole, J. M. Lincecum, K. Thompson, N. Kelly, A. Bostrom, J. Theodoss, B. M. Al-Nakhala, F. G. Vieira, J. Ramasubbu, J. A. Heywood, Design, power, and interpretation of studies in the standard murine model of ALS. *Amyotroph. Lateral Scler.* **9**, 4–15 (2008).
34. A. Gill, J. Kidd, F. Vieira, K. Thompson, S. Perrin, No benefit from chronic lithium dosing in a sibling-matched, gender balanced, investigator-blinded trial using a standard mouse model of familial ALS. *PLOS ONE* **4**, e6489 (2009).
35. R. M. Koffie, M. Meyer-Luehmann, T. Hashimoto, K. W. Adams, M. L. Mielke, M. Garcia-Alloza, K. D. Micheva, S. J. Smith, M. L. Kim, V. M. Lee, B. T. Hyman, T. L. Spires-Jones, Oligomeric amyloid β associates with postsynaptic densities and correlates with excitatory synapse loss near senile plaques. *Proc. Natl. Acad. Sci. U.S.A.* **106**, 4012–4017 (2009).
36. J. E. Hanson, W. J. Meilandt, A. Gogineni, P. Reynen, J. Herrington, R. M. Weimer, K. Scearce-Levie, Q. Zhou, Chronic GluN2B antagonism disrupts behavior in wild-type mice without protecting against synapse loss or memory impairment in Alzheimer's disease mouse models. *J. Neurosci.* **34**, 8277–8288 (2014).
37. T. Bittner, M. Fuhrmann, S. Burgold, S. M. Ochs, N. Hoffmann, G. Mitteregger, H. Kretzschmar, F. M. LaFerla, J. Herms, Multiple events lead to dendritic spine loss in triple transgenic Alzheimer's disease mice. *PLOS ONE* **5**, e15477 (2010).
38. T. A. Lanz, D. B. Carter, K. M. Merchant, Dendritic spine loss in the hippocampus of young PDAPP and Tg2576 mice and its prevention by the ApoE2 genotype. *Neurobiol. Dis.* **13**, 246–253 (2003).
39. T. L. Spires-Jones, M. Meyer-Luehmann, J. D. Osetek, P. B. Jones, E. A. Stern, B. J. Bacskai, B. T. Hyman, Impaired spine stability underlies plaque-related spine loss in an Alzheimer's disease mouse model. *Am. J. Pathol.* **171**, 1304–1311 (2007).
40. M. C. Irizarry, M. McNamara, K. Fedorchak, K. Hsiao, B. T. Hyman, APPsw transgenic mice develop age-related Aβ deposits and neuropil abnormalities, but no neuronal loss in CA1. *J. Neuropathol. Exp. Neurol.* **56**, 965–973 (1997).
41. M. C. Irizarry, F. Soriano, M. McNamara, K. J. Page, D. Schenk, D. Games, B. T. Hyman, Aβ deposition is associated with neuropil changes, but not with overt neuronal loss in the human amyloid precursor protein V717F (PDAPP) transgenic mouse. *J. Neurosci.* **17**, 7053–7059 (1997).
42. S. T. DeKosky, S. W. Scheff, Synapse loss in frontal cortex biopsies in Alzheimer's disease: Correlation with cognitive severity. *Ann. Neurol.* **27**, 457–464 (1990).
43. R. D. Terry, E. Masliah, D. P. Salmon, N. Butters, R. DeTeresa, R. Hill, L. A. Hansen, R. Katzman, Physical basis of cognitive alterations in Alzheimer's disease: Synapse loss is the major correlate of cognitive impairment. *Ann. Neurol.* **30**, 572–580 (1991).
44. S. H. Lee, C. E. Le Pichon, O. Adolfsson, V. Gafner, M. Pihlgren, H. Lin, H. Solanoy, R. Brendza, H. Ngu, O. Foreman, R. Chan, J. A. Ernst, D. DiCara, I. Hotzel, K. Srinivasan, D. V. Hansen, J. Atwal, Y. Lu, D. Bumbaca, A. Pfeifer, R. J. Watts, A. Muhs, K. Scearce-Levie, G. Ayalon, Antibody-mediated targeting of tau in vivo does not require effector function and microglial engagement. *Cell Rep.* **16**, 1690–1700 (2016).
45. C. E. Le Pichon, S. L. Dominguez, H. Solanoy, H. Ngu, N. Lewin-Koh, M. Chen, J. Eastham-Anderson, R. Watts, K. Scearce-Levie, EGFR inhibitor erlotinib delays disease progression but does not extend survival in the SOD1 mouse model of ALS. *PLOS ONE* **8**, e62342 (2013).
46. S. Pun, A. F. Santos, S. Saxena, L. Xu, P. Caroni, Selective vulnerability and pruning of phasic motoneuron axons in motoneuron disease alleviated by CNTF. *Nat. Neurosci.* **9**, 408–419 (2006).
47. S. Huntwork-Rodriguez, B. Wang, T. Watkins, A. Sengupta Ghosh, C. D. Pozniak, D. Bustos, K. Newton, D. S. Kirkpatrick, J. W. Lewcock, JNK-mediated phosphorylation of DLK suppresses its ubiquitination to promote neuronal apoptosis. *J. Cell Biol.* **202**, 747–763 (2013).
48. M. Mata, S. E. Merritt, G. Fan, G. G. Yu, L. B. Holzman, Characterization of dual leucine zipper-bearing kinase, a mixed lineage kinase present in synaptic terminals whose phosphorylation state is regulated by membrane depolarization via calcineurin. *J. Biol. Chem.* **271**, 16888–16896 (1996).
49. S.-i. Hirai, A. Kawaguchi, J. Suenaga, M. Ono, D. F. Cui, S. Ohno, Expression of MUK/DLK/ZPK, an activator of the JNK pathway, in the nervous systems of the developing mouse embryo. *Gene Expr. Patterns* **5**, 517–523 (2005).
50. K. Srinivasan, B. A. Friedman, J. L. Larson, B. E. Lauffer, L. D. Goldstein, L. L. Appling, J. Borneo, C. Poon, T. Ho, F. Cai, P. Steiner, M. P. van der Brug, Z. Modrusan, J. S. Kaminker, D. V. Hansen, Untangling the brain's neuroinflammatory and neurodegenerative transcriptional responses. *Nat. Commun.* **7**, 11295 (2016).

Acknowledgments: We thank J. C. Cox and M. Martinez for performing the SOD1 copy number variation assay; G. Deshmukh for help generating the pharmacokinetic/pharmacodynamic model and pharmacokinetic study support; A. Sambrone for DLK inhibitor formulations; T. Earr for assistance with dosing and tissue collection; Z. Sheng for muscle sectioning and staining; M. G. Edick and J. Eastham-Anderson for managing histopathology workflow; A. Jubb for analyzing histopathology in human AD samples; K. Stark for obtaining GNE-3511–medicated mouse chow; B. Forrest for assistance with statistical analysis; and G. Ayalon, T. Yuen, and S. Huntwork-Rodriguez for helpful comments. **Funding:** All experiments were funded by Genentech, except for the Western blot of ALS patient and control spinal cord tissues, which was funded by the following grants to E.J.H.: NIH R01NS098516-02 and Department of Veterans Affairs Merit Awards I01 RX002213-02 and I01 BX001108-06. **Author contributions:** C.E.L.P., K.S.-L., and J.W.L. designed the $SOD1^{G93A}$ mouse model experiments. W.J.M., R.W., R.A.D.C., K.S.-L., and J.W.L. designed the PS2APP and Tau experiments. Y.R. and J.W.L. designed the in vitro motor neuron experiments. E.J.H. and J.W.L. designed the experiment investigating ALS patient tissue, and S.L. performed it. C.E.L.P., S.D., H.L., C.D.P., X.L., and M.B. performed and analyzed the experiments using $SOD1^{G93A}$ mice. W.J.M., H.S., A. Gogineni, S.-H.L, J.M., and V.D.G. performed and analyzed the experiments using PS2APP and Tau mice. H.S., A.S.G., Z.J., B.W., and A. Gustafson performed and analyzed the optic nerve crush experiments. S.-H.L. and W.J.M. performed and analyzed the experiments using AD tissue. H.N. performed image analysis of all the histology across studies. O.F. analyzed the early AD and AD patient tissue histology. Y.R. performed and analyzed the in vitro motor neuron experiments. S.P. and M.S. produced DLK inhibitors and contributed to the analysis of experiments using the inhibitors. Z.M. and J.K. performed and analyzed the RNA-seq experiment. C.E.L.P., W.J.M., K.S.-L., and J.W.L. wrote the manuscript. **Competing interests:** All authors were employees of Genentech during the course of these studies, except for S.L., Y.R., and E.J.H. M.S. and S.P. are co-inventors on two patents related to the drugs used in this study: Patent #WO 2013174780 entitled "Preparation of substituted dipyridylamines as DLK inhibitors for treating neurodegeneration" (2013) and Patent #WO 2014111496 entitled "Preparation of pyrazolylpyridinamine derivatives for use as DLK inhibitors" (2014). **Data and materials availability:** Data obtained in the RNA-seq study has been deposited to the Gene Expression Omnibus database (GSE96592). Requests for materials can be sent to the Genentech Outgoing Material Transfer agreements program (www.gene.com/scientists/mta).

Submitted 4 May 2016
Resubmitted 23 November 2016
Accepted 27 March 2017
Published 16 August 2017
10.1126/scitranslmed.aag0394

Citation: C. E. Le Pichon, W. J. Meilandt, S. Dominguez, H. Solanoy, H. Lin, H. Ngu, A. Gogineni, A. Sengupta Ghosh, Z. Jiang, S.-H. Lee, J. Maloney, V. D. Gandham, C. D. Pozniak, B. Wang, S. Lee, M. Siu, S. Patel, Z. Modrusan, X. Liu, Y. Rudhard, M. Baca, A. Gustafson, J. Kaminker, R. A. D. Carano, E. J. Huang, O. Foreman, R. Weimer, K. Scearce-Levie, J. W. Lewcock, Loss of dual leucine zipper kinase signaling is protective in animal models of neurodegenerative disease. *Sci. Transl. Med.* **9**, eaag0394 (2017).

Science Translational Medicine

Loss of dual leucine zipper kinase signaling is protective in animal models of neurodegenerative disease

Claire E. Le Pichon, William J. Meilandt, Sara Dominguez, Hilda Solanoy, Han Lin, Hai Ngu, Alvin Gogineni, Arundhati Sengupta Ghosh, Zhiyu Jiang, Seung-Hye Lee, Janice Maloney, Vineela D. Gandham, Christine D. Pozniak, Bei Wang, Sebum Lee, Michael Siu, Snahel Patel, Zora Modrusan, Xingrong Liu, York Rudhard, Miriam Baca, Amy Gustafson, Josh Kaminker, Richard A. D. Carano, Eric J. Huang, Oded Foreman, Robby Weimer, Kimberly Scearce-Levie and Joseph W. Lewcock

Sci Transl Med **9**, eaag0394.
DOI: 10.1126/scitranslmed.aag0394

A new therapeutic target zips into view

The genetics, pathology, and clinical manifestations of chronic neurodegenerative diseases, such as amyotrophic lateral sclerosis (ALS), are heterogeneous, which has made the development and testing of candidate therapeutics difficult. Here, Le Pichon *et al*. identify dual leucine zipper kinase (DLK) as a common regulator of neuronal degeneration in mouse models of ALS and Alzheimer's disease and in human patient postmortem brain tissue. Deletion of DLK or treatment with a DLK inhibitor resulted in neuronal protection and slowing of disease progression after diverse insults in several mouse models of neurodegenerative disease. This suggests that DLK may have broad applicability as a therapeutic target for the treatment of a number of neurodegenerative diseases.